Geomechanics and Engineering, *Vol. 36, No. 3 (2024) 277-293*
https://doi.org/10.12989/gae.2024.36.3.277

Seismic fragility assessment of shored mechanically stabilized earth walls

Sheida Ilbagitaher[1a] and Hamid Alielahi*[2]

[1]*Department of Civil Engineering, University of Science and Culture, Tehran, Iran*
[2]*Department of Civil Engineering, Zanjan Branch, Islamic Azad University, Zanjan, Iran*

(*Received June 13, 2023, Revised October 12, 2023, Accepted January 8, 2024*)

Abstract. Shored Mechanically Stabilized Earth (SMSE) walls are types of soil retaining structures that increase soil stability under static and dynamic loads. The damage caused by an earthquake can be determined by evaluating the probabilistic seismic response of SMSE walls. This study aimed to assess the seismic performance of SMSE walls and provide fragility curves for evaluating failure levels. The generated fragility curves can help to improve the seismic performance of these walls through assessing and controlling variables like backfill surface settlement, lateral deformation of facing, and permanent relocation of the wall. A parametric study was performed based on a non-linear elastoplastic constitutive model known as the hardening soil model with small-strain stiffness, HSsmall. The analyses were conducted using PLAXIS 2D, a Finite Element Method (FEM) program, under plane-strain conditions to study the effect of the number of geogrid layers and the axial stiffness of geogrids on the performance of SMSE walls. In this study, three areas of damage (minor, moderate, and severe) were observed and, in all cases, the wall has not completely entered the stage of destruction. For the base model (Model A), at the highest ground acceleration coefficient (1 g), in the moderate damage state, the fragility probability was 76%. These values were 62%, and 54%, respectively, by increasing the number of geogrids (Model B) and increasing the geogrid stiffness (Model C). Meanwhile, the fragility values were 99%, 98%, and 97%, respectively in the case of minor damage. Notably, the probability of complete destruction was zero percent in all models.

Keywords: dynamic analysis; fragility curves; numerical method; seismic performance; Shored Mechanically Stabilized Earth (SMSE) wall

1. Introduction

In recent decades, the construction of Mechanically Stabilized Earth (MSE) walls with geosynthetic layers has received much attention, especially in the development of transportation networks such as highways, railways, bridge piles, and other retaining walls in the vicinity of urban buildings. Since Vidal introduced reinforced retaining wall technology in 1966, many researchers have focused on reinforced retaining wall technology. Compared to traditional retaining walls, reinforced retaining wall has the advantages of simple construction, suitable flexibility, high seismic resistance, and economic efficiency (Berg *et al*. 2009). However, according to the recommendations and guidelines for reinforced soil walls, to meet the geotechnical design needs, the length of the reinforcement elements should not be less than 0.7 H (H: the height of the wall) (Morrison *et al.* 2006), which can lead to excessive ground occupation, especially in places with limited access. For this reason, Shored Mechanically Stabilized Earth (SMSE) walls were proposed by Morrison (2006) Fig. 1(a).

Given the complex topography, sloping terrain, and the space limitation for construction in mountainous areas, the use of SMSE walls has become more prominent. Experiences from implementing SMSE walls to widen or construct new roads show their proper performance, especially in mountain roads. In addition, SMSE walls are capable of supporting vehicle traffic during construction. SMSE walls are new retaining wall technology in which three main elements of reinforcing elements (including polymer networks such as geogrid or geotextile layers), compact embankment, and shoring systems are used. Using SMSE walls has some advantages such as flexibility against subgrade settlement, higher stability and safety against earthquakes, and economic efficiency. In order to fully understand the economic and technological benefits of SMSE walls, it is crucial to describe how these structures behave under seismic loads.

When an area is affected by an earthquake or seismic sequences, access to this area becomes more difficult considering the damages in airports, sea ports, etc. This reveals the importance of the safety of road networks and their main components (like bridges, retaining structures, tunnels, etc.).In this regard, earth-retaining structures along roadways are critical infrastructure components that can sustain severe damage in a seismic event. Experience from past earthquakes has shown that the seismic vulnerability of retaining walls has caused great economic losses. The performance of reinforced soil walls due to major earthquakes such as the Northridge earthquake in the United States (1994), the Kobe earthquake (1995), and the Niigata

*Corresponding author, Assistant Professor, Ph.D.
E-mail: ha.alielahi@iau.ac.ir; h.alielahi@gmail.com
[a]MSc
E-mail: sh.ilbagitaher@gmail.com

http://www.techno-press.org/?journal=gae&subpage=7
ISSN: 2005-307X (Print), 2092-6219 (Online)

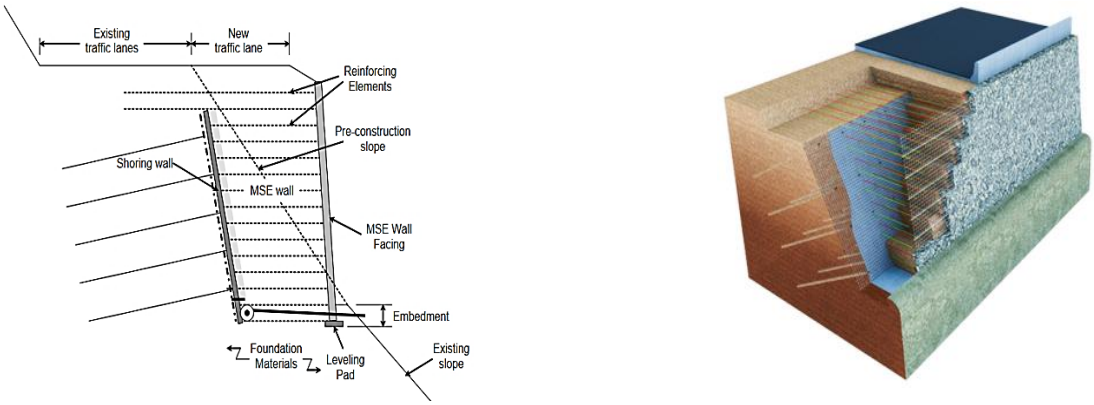

(a) (b)

Fig. 1 (a) Generic cross-section of an SMSE wall system (Morrison *et al*. 2006) and (b) 3D view of SMSE wall system

earthquake in Japan (2004) showed the proper performance of this type of wall compared to other retaining structures. However, some reports showed various types of failure in soil reinforcement systems (Morrison *et al.* 2006). Due to the greater performance of MSE and reinforced earth walls compared to conventional retaining walls, particularly in earthquake-prone areas, the seismic behavior of these walls has been the subject of extensive investigation (e.g., Xu *et al.* 2021 a, b, Xu *et al.* 2020, Turkel *et al.* 2020, Yazdandoust 2017; Jiang *et al.* 2016, Xie and Leshchinsky 2015, Alhabshi 2006, Sutani *et al.* 2005, Sandri 1994, Hamrouni *et al*. 2018, Altay *et al.* 2021, Hamrouni *et al.* 2021). It is worth noting that research on MSE walls subjected to static loads has grown significantly. However, studies on the seismic response of such walls under dynamic loads have not yet matured sufficiently to provide a suitable framework for seismic design. The following gives a brief overview of the most significant numerical and experimental studies in this field:

After the Kobe earthquake, Tatsuko *et al.* (1995) analyzed the behavior of a 6.2-meter-high MSE wall with geosynthetic and found that there were no signs of cracking or damage in the wall. Ling *et al.* (2001) studied the Chi-Chi earthquake on six MSE walls and reported that most of the damage was due to the lack of seismic design in the structure. The shaking table test results by El-Imam and Bathurst (2006) illustrated that by increasing the stiffness of the reinforcements, the lateral displacement of the wall decreases sharply. Also, the forces acting on the wall and the reinforcements are strongly influenced by the reinforcing layers arrangement, reinforcement type, and the distance between them. Furthermore, Yuu *et al.* (2008) by using a shaking table test showed that MSE walls reinforced by geocells fail under cyclic or transient short-time seismic loads. This study represented that MSE walls reinforced by geocell have sufficient flexibility to withstand large deformations and have a high resistance under seismic load.

The results of the shaking table test and numerical studies by Yazdandoust (2019) on the seismic performance of a combined MSE wall system showed that the length of nail elements and geogrid elements in the composite system as a wall's height factor could be introduced as an efficient arrangement. Safaee *et al.* (2021), by studying the seismic performance of the single-layer and multi-layer MSE walls using physical modeling and shaking table tests, found that layered walls (multi-layer) have better performance in terms of seismic stability, wall crown displacement, horizontal displacement of the shoring wall, deformation mode, and wall failure mechanism. Also, the results of Kamalzadeh and Pender's numerical study (2022) illustrated that the MSE wall with a 6-meters-length geogrid behaves similarly to a rigid block with no apparent relative displacement or lateral strain inside the block when subjected to 5-pulse Ricker wavelet input scaled to 0.15 g. Xu *et al.* (2023) investigated the influence of reinforcement arrangement on the dynamic response of MSE walls. The results show that placing longer reinforcement layers at the top of the wall can improve its seismic stability. Zheng *et al.* (2023) carried out an experimental study on back-to-back MSE walls with shaking table tests and concluded that incremental reinforcement tensile strains increase significantly with rising input acceleration.

As previously mentioned, the SMSE walls have superior advantages over MSE walls because of the shoring system. Morrison *et al.* (2006) published a guideline book for designing MSE walls based on the FHWA, which introduced the new design criteria using three methods: field tests, a centrifuge model test, and a numerical static analysis. The results showed that the use of an MSE wall with a shoring wall system significantly reduced the lateral deformations compared to a conventional wall. A geotechnical centrifuge test was carried out by Lee *et al.* (2010) for the SMSE wall under surcharge loading to investigate the deformation of the wall. The surcharge loads application was observed to affect only the deformation response of the wall's upper part, and the maximum lateral face displacement occurred at the mid-height of the wall. Based on the limit equilibrium method, Yang *et al.* (2011) investigated the failure surfaces of SMSE walls that were related to the size of L/H (L and H refer to the reinforcement length and the wall height, respectively). When L/H = 0.6, there was a slight difference between the numerical and test results, and the failure surface was in the transition from the "double-line" type to the "single-line" type. Ren *et al.* (2019) by comparing the results of the model test and the numerical simulation of the SMSE wall,

demonstrated that the restraints (anchors) in the connected system could reduce the lateral pressure and improve the stability of the SMSE wall. Moreover, the main factor in the difference between the results of the full-scale model and the reduced-scale model was expressed by gravity. Several large-scale model tests were conducted by Ren *et al.* (2022) to explore the mechanical behavior of composite structures with different connection forms and relative densities. The results showed that the deformation of SMSE walls is mainly concentrated in the upper middle part, showing a "bulging" failure trend.

Considering prior studies, most of them have focused on the behavior of MSE walls and few have been conducted on SMSE walls. Also, they were mostly limited to static loading conditions and research on the behavior of MSE walls for dynamic loading is limited and fragility curves for seismic evaluation of MSE walls have not been provided. Similarly, recent investigations were only limited to static loading on SMSE walls, and very few dynamic studies and seismic vulnerability assessments have been conducted on the SMSE walls. However, to characterize the seismic performance of retaining structures and have an economical design in engineering practice, a more comprehensive damage control should be included rather than just relying on the ultimate state. to achieve this, the performance-based design approach has been integrated with the probabilistic framework as a useful tool for conducting the vulnerability assessments and damage analyses necessary for managing seismic risk in transportation infrastructures. In this regard, fragility curves have been widely used for seismic risk evaluation helping to link economic loss to structural system damage. Unlike an extensive amount of seismic risk evaluating different waterfront quay walls (Alielahi and Rabeti Mogadam 2017, Jafarian and Miraei 2019), limited research has been devoted to fragility evaluating the earth-retaining walls that are mostly related to gravity walls (Huang *et al.* 2018, Alainia 2019, Cosentini and Bozzoni 2022), cantilever walls (Argyroudis *et al.* 2013, Zamiran and Osouli 2018), and soil nail walls (Bayat *et al.* 2021).

Previous studies on MSE walls were mostly limited to static studies and research on the behavior of MSE walls for dynamic loading conditions is limited. Also, fragility curves for seismic evaluation of MSE walls are not provided. Recent research was only limited to static studies on SMSE walls, and no dynamic studies and seismic vulnerability have been conducted on the SMSE walls. Therefore, more study is needed to investigate the dynamic behavior of SMSE walls and provide fragility curves. Results from this study provide insights into the dynamic response and the seismic vulnerability by extracting the seismic analytical fragility curves of SMSE walls, which can help the safe design of infrastructure and protect lives in earthquake-prone regions.

Therefore, as the main objective of the current study, the seismic vulnerability of SMSE walls was investigated by providing the seismic fragility curves based on the analytical method. To achieve this, a series of non-linear finite element numerical models have been developed using PLAXIS 2D, and the HS-small soil model has been implemented to evaluate the dynamic behavior of the SMSE walls rigorously. In addition, the number and stiffness of geogrids were increased in different analyses models, and the obtained results were compared. Eventually, damage probabilities were evaluated by considering three damage states including minor, moderate, and extensive for various ground motion intensities.

2. Numerical modeling

In the current study, a finite-element-based program, PLAXIS 2D (V.2020), was used to develop a plane-strain model to perform the dynamic analysis of the SMSE walls subjected to earthquake motions. According to Fig. 2, the SMSE wall was modeled on a layer of poorly graded sand (Foundation) with a height of 8 m. A retaining wall with 6 m of height (H= 6 m) was considered, while the slope rate of the retaining wall was 1:0.25. The FHWA recommended length of the reinforcements (geogrids) for this type of wall should be equal to three-tenths of the wall's height (0.3H= 1.8 m), and the length of the restraints (anchors) should be six-tenths of the wall's height (0.6H=3.6 m) (Morrison *et al.* 2006). As the main focus of this study is on the overall dynamic behavior of SMSE wall system, the time-dependency effects of creep on geogrid strength and stiffness are not taken into consideration. To prevent the impact of lateral boundaries on the results of seismic analysis, in addition to the free field absorber boundary, the existing natural soil behind the SMSE wall was modeled with a sufficient distance. It should be noted that the distance between the wall and boundary conditions is chosen based on trial and error method through checking the displacement differences between sequential steps till it reached below 1% on wall's both sides and has been selected between 2H to 3H as an optimal boundary distance (Wood, 2004). A poorly graded sand with C_u= 1.87, C_c= 1.02, maximum and minimum void ratios of 0.85 and 0.51, respectively, and a relative density of 86% was used as the backfill soil in the model (Ren *et al.* 2019). In addition, stainless-steel threads were used in five layers to simulate the anchors in the back slope. 15-noded triangular elements were used for soil modeling, the reinforcement elements were used for geogrids modeling, and the node-to-node anchor was adopted to simulate the anchors. In order to ensure accuracy, the meshes surrounding the reinforcement elements were refined. In addition, interface elements were set among the reinforcement, the back slope surface, and the filling soil. The linear elastic model with the Mohr-Coulomb failure criterion was employed to represent the frictional interfaces. Additionally, there is interlocking between soil and geogrids because of frictional interactions and for this reason, the SMSEW was modeled with rigid interfaces to prevent separation or sliding (fully-bonded interfaces were accounted with a value of R_{int} = 1.0) (PLAXIS 2D Reference Manual 2020, Kamalzadeh and Pender 2023). Since evaluating wall deformation is important, the HS small soil model was adopted for the soil (PLAXIS 2D Reference Manual 2020, Deghoul *et al.* 2020), and an elastic model was used for the reinforcements given their small deformation. Besides, in the modeling, a

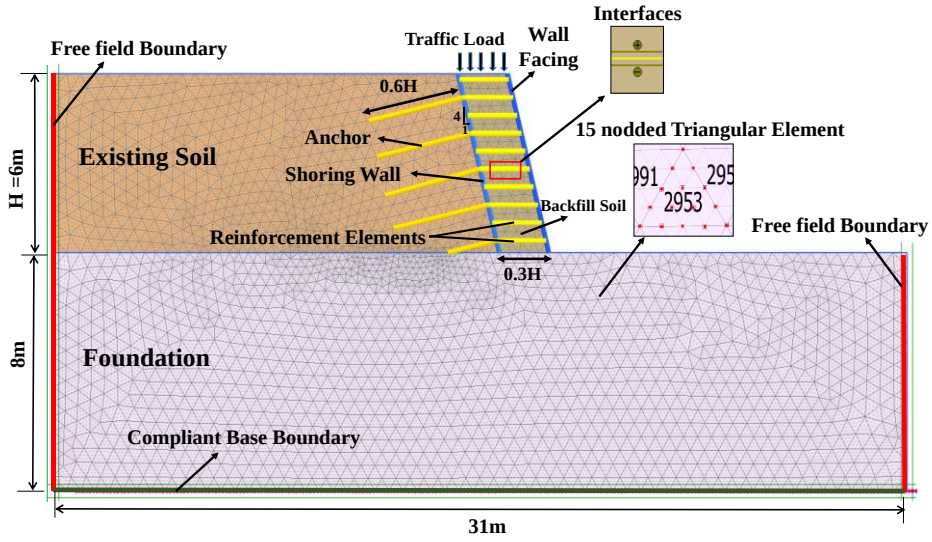

Fig. 2 Geometry, meshing, and wall boundaries of the numerical model (all sizes are in meters)

Table 1 Material properties (Ren *et al.* 2019)

Material	Axial stiffness *EA*, kN.m^{-1}	Flexural stiffness *EI*, kN.m^2/m
Reinforcement (Geogrid)	3500	-
Anchor	1×10^7	-
Loading plate	1.5×10^7	2.7×10^5

Table 2 Soils properties and behavioral model (HS small model parameters)

Parameter	Symbol	Backfill soil	Foundation material
Model	-	HSsmall	HSsmall
Unit weight, (kN · m^{-3})	γ	16.7	25.8
Secant stiffness in standard drained triaxial test (kN/m^2)	E_{50}^{ref}	3.5×10^6	1×10^6
Tangent stiffness for primary oedometer loading (kN/m^2)	E_{oed}^{ref}	3.5×10^6	1×10^6
Unloading/reloading stiffness from drained triaxial test (kN/m^2)	E_{ur}^{ref}	10.5×10^6	3×10^6
Poisson's ratio for unloading-reloading	$\nu_{0.7}$	0.35	0.22
Cohesion, (kPa)	C	8	200
Internal friction angle, (°)	ϕ	30	52
Reference shear modulus at very small strains ($\varepsilon<10^{-6}$) (kN/m^2)	G_0^{ref}	10.8×10^6	3.1×10^6
Threshold shear strain at which ($G_s = 0.722G_0$)	$\gamma_{0.7}$	2×10^{-4}	2×10^{-4}
Reference pressure for stiffness (kPa)	P_{ref}	100	100

traffic load of 70 kPa is taken into account on the top of the SMSE wall. The values of the relevant parameters are obtained from the experimental tests by Ren and Qi (2017) and Zhang (2017) and are provided in Tables 1 and 2.

A standard absorbent boundary was applied to the model for dynamic analysis (PLAXIS 2D Reference Manual 2020). The free field boundary condition was used for both vertical sides of the model to prevent the reflection of waves in dynamic analysis and absorb the waves propagating from the earthquake's source. The compliant base boundary has been applied with a prescribed horizontal displacement for the bottom of the model. The use of prescribed displacements permits the application of time histories of displacements, velocity, or acceleration during the calculation phase (Fig. 2).

In the numerical model, the size of the mesh discretization in the dynamic analysis is important to ensure proper wave propagation through the model. The maximum element size can be calculated according to Kuhlemeyer and Lysmer (1973). ΔL is defined as

$$\Delta L \leq \frac{\lambda}{8} = \frac{V_s}{8 f_{max}} \quad (1)$$

The maximum spatial element size must be smaller than one-tenth to one-eighth of the λ (Wavelength) associated with the V_s (Shear wave velocity) and the highest frequency component of the input motion (f_{max}).

3. Validation of the numerical model

The review of the literature indicated that there is no study on the seismic behavior of SMSE walls, and most studies focused on their static behavior. Therefore, model validation was performed based on Ren *et al.*'s (2019) research available in the literature. Ren *et al.*'s study is a full-scale numerical simulation based on static behavior for SMSE walls and the results of a reduced-scale model (Ren and Qi 2017, Zhang 2017). The results of these models, reduced-scale and full-scale, were compared and analyzed.

In this study, a full-scale numerical model was used, and in the following, only the dynamic behavior of the SMSE wall was investigated.

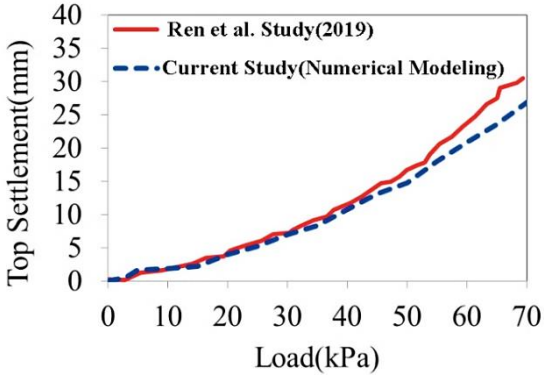

Fig. 3 The result of SMSE wall surface settlement (load-settlement)

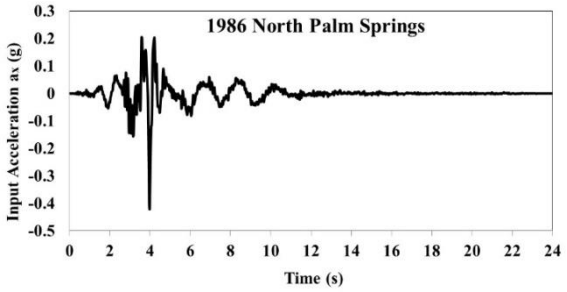

(a) North Palm Springers

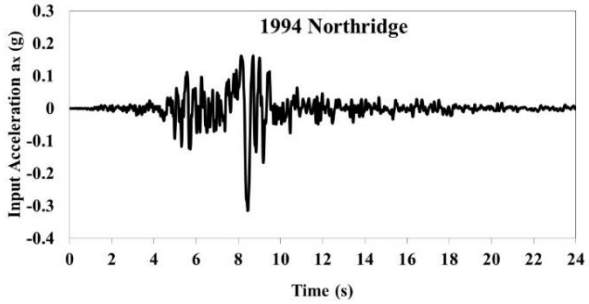

(b) Northridge

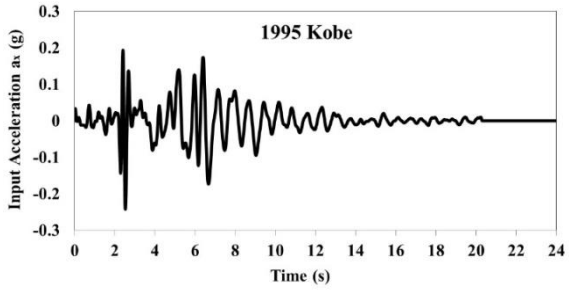

(c) Kobe

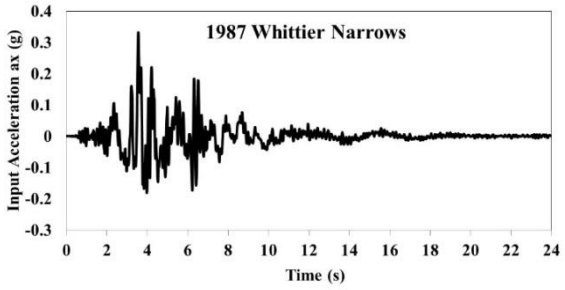

(d) Whittier Narrows

Fig. 4 Four input earthquake motions in parametric analysis

Fig. 3 shows the comparison between the results from the present model and the measured displacement at the wall height under the traffic load of 70 kPa. According to the studies of Ren *et al*. (2019), the settlement of the wall surface under a load of 70 kPa is calculated at about 30.5 mm, which was about 27 mm for the HSsmall behavioral model. Also, the maximum horizontal displacement is distributed at the height of 1 to 5 meters (Ren *et al*. 2019), which was 1.5 to 5 meters for the HSsmall model that shows acceptable compliance. Through the validation assessment, it can be inferred that the results from the numerical model of the present study are in a reasonable agreement with the measured displacements from the full-scale testing, although only static results were given for the SMSE wall. Considering this, the behavioral model of HSsmall was used for dynamic analysis.

4. Dynamic behavior of SMSE walls

First, by considering the study of Ren *et al.* (2019), the wall was modeled statically and used as the basis of dynamic studies due to the lack of dynamic studies on this type of wall. The two–dimensional plane strain dynamic

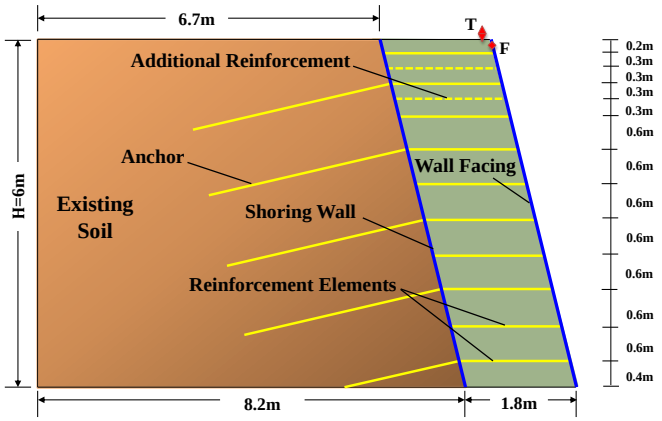

Fig. 5 Schematic figure of SMSE wall's dimensions and geogrids arrangements (all sizes are in meters)

implicit method was applied for the numerical analysis of an SMSE wall using the PLAXIS 2D finite element software.

In the section on parametric studies, by changing a parameter in a specific range or to a certain extent, its effect on the lateral displacement of the facing and displacement of the embankment surface with the approach of improving the performance level is investigated. The effect of the earthquake on the SMSE wall system is simulated by applying a horizontal acceleration time history at the base of the FE model. Four time histories of previous earthquakes including Kobe (1995), Whittier Narrows (1987), North Palm Springs (1986), and Northridge (1994) events have been employed (Fig. 4). The ground motions used for parametric studies are obtained from the Pacific Earthquake Engineering Research Center website (PEER ground motion database). Also, more information about these ground motions is provided in Table 3. The stages of construction and loading were defined according to the conditions of the study and then analyzed. For the dynamic analysis of the wall, stage construction mode with 11 stages was activated and then earthquake records were applied to the wall in the final phase.

Based on previous studies on reinforced retaining walls with geogrids, three effective factors in the horizontal and vertical displacement of these walls include the number, stiffness, and length of geogrids. Since the length of geogrids in the SMSE walls is limited because of the shoring wall and reinforcements, therefore, in this paper, the parameters that were studied in the dynamic analysis were:

- Increasing the number of geogrids (reducing the distance between geogrids)
- Increasing the axial stiffness of geogrids

In this study, the basic model, the model by increasing the number of geogrids, and the model by increasing the axial stiffness of geogrids have been shown with Model A, Model B, and Model C, respectively.

4.1 Dynamic analysis results

Analysis of the base model under dynamic conditions showed that major deformations occur in the crown of the SMSE wall (Point T). Furthermore, based on the models studied in the FHWA design guidelines (Morrison *et al.* 2006), two additional geogrids have been used in the upper layers of the wall (Model B) Fig. 5. Also, its effect on the seismic behavior of these walls has been investigated. As mentioned before, another effective parameter in reducing horizontal displacement and top settlement of the MSE walls is increasing the stiffness of the reinforcements. Therefore, in Model C the axial stiffness of the geogrids has been increased (up to double), and the model has been investigated in dynamic conditions under selected earthquakes for a new state. Fig. 6 shows the top settlement (Point T) for dynamic conditions in the four selected earthquakes.

As can be observed in Fig. 6, the top settlement of the wall (Point T) is reduced by about 9 to 21% in Model B and 24 to 43% in Model C, compared to Model A. Moreover, the maximum settlements in the SMSE wall which are equal to 37 mm for Model A, as well as 29 mm for Model B (18% reduction) and 23 mm for Model C (43% reduction) occurred in the Northridge earthquake. According to the results Fig. 7, it can be mentioned that increasing the number of geogrids (reducing the distance between geogrids) is effective in reducing the wall's settlement (an average of 16% reduction in settlement) and improves the efficiency of the wall under seismic loading due to more interlock of geogrid networks with soil and their high rigidity. Furthermore, increasing the stiffness of geogrids is effective in reducing wall settlement (on average of 34% reduction in settlement) and improves the efficiency of the wall under seismic loads. Fig. 8 illustrates the maximum horizontal displacement of the wall.

As shown in Fig. 8, the maximum horizontal displacement of the wall is reduced in Models B and C under static and dynamic loading conditions. The former is about 12 to 19% and the latter is 12 to 22% in dynamic analysis. Note that these values in static conditions are 8% and 20%, respectively. As expected, the Northridge earthquake caused the largest horizontal displacement in the SMSE wall with a value of 57 mm for Model A, 47 mm for Model B (17% reduction), and 46 mm for Model C (19% reduction). In addition, the horizontal displacement of the

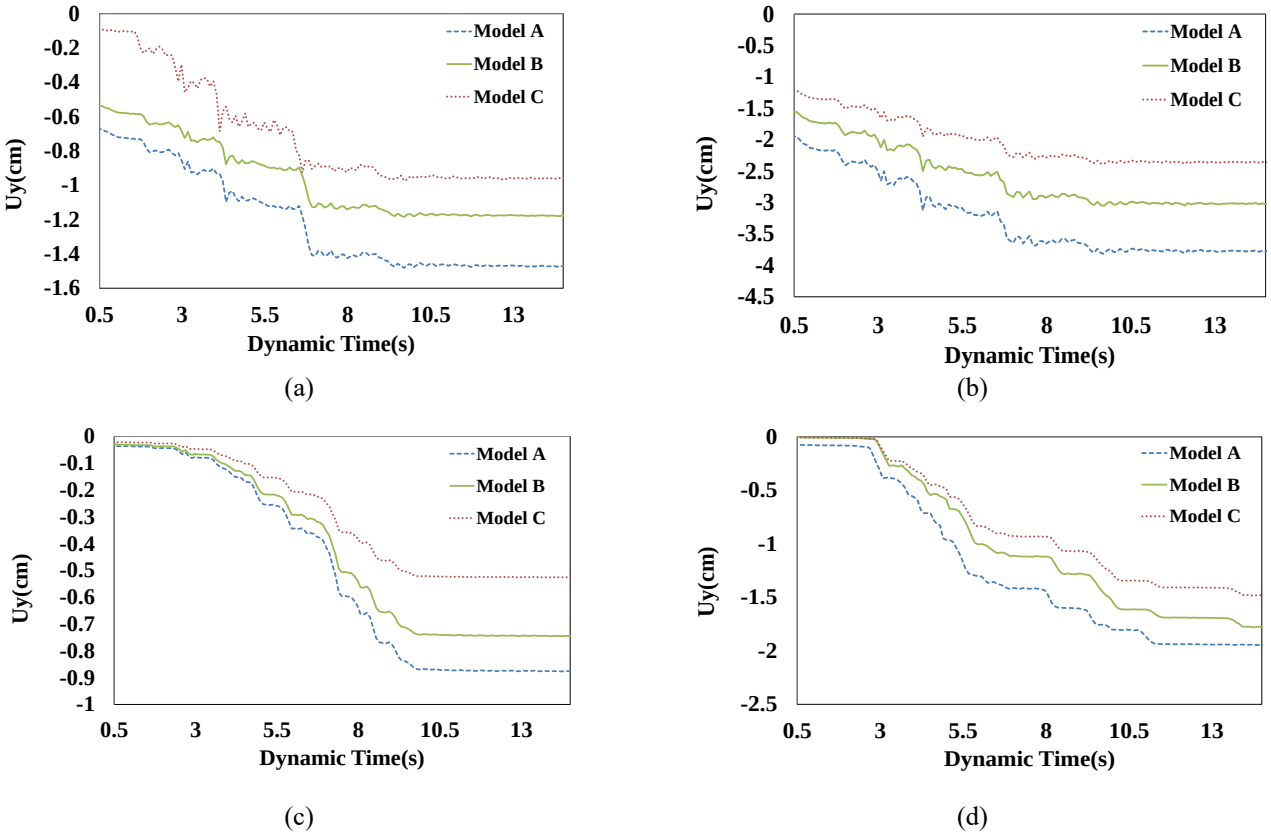

Fig. 6 Comparison of top residual settlement (Point T) between Model A: Base model, Model B: Increased geogrids number model and Model C: Increased geogrids stiffness model in the (a) North Palm Spring, (b) Northridge, (c) Kobe and (d) Whittier Narrow earthquakes

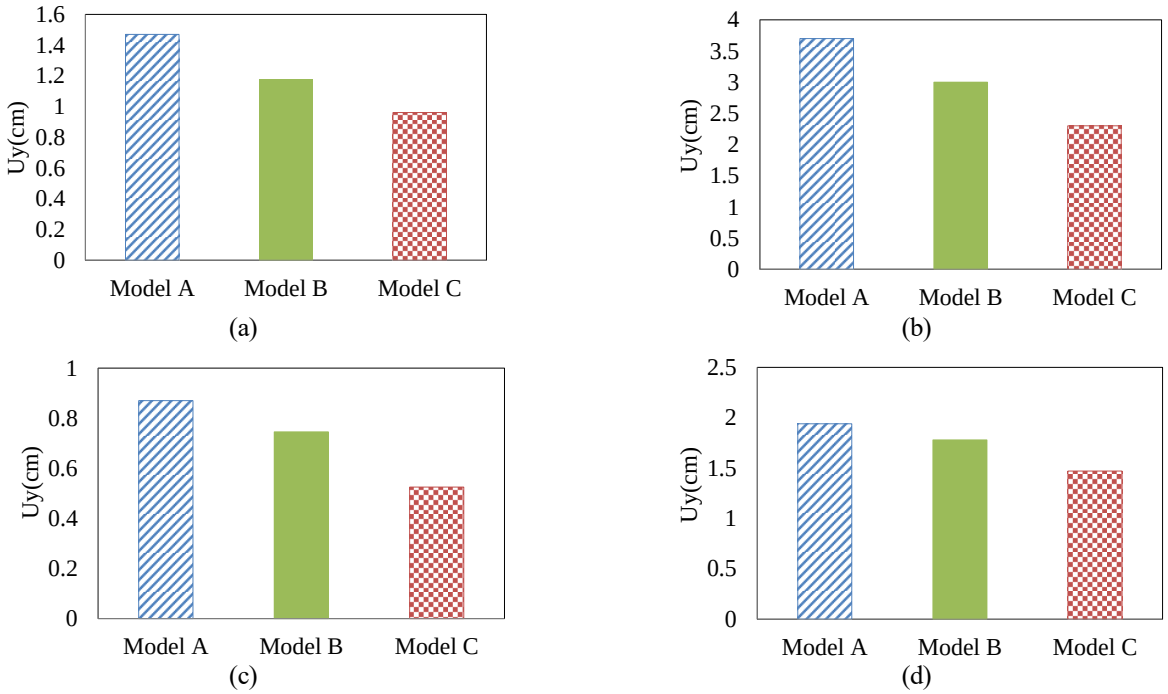

Fig. 7 Bar graphs of SMSEW top residual settlement (Point T) in the (a) North Palm Spring, (b) Northridge, (c) Kobe and (d) Whittier Narrow earthquakes (Model A: Base model, Model B: Increased geogrids number model, and Model C: Increased geogrids stiffness model)

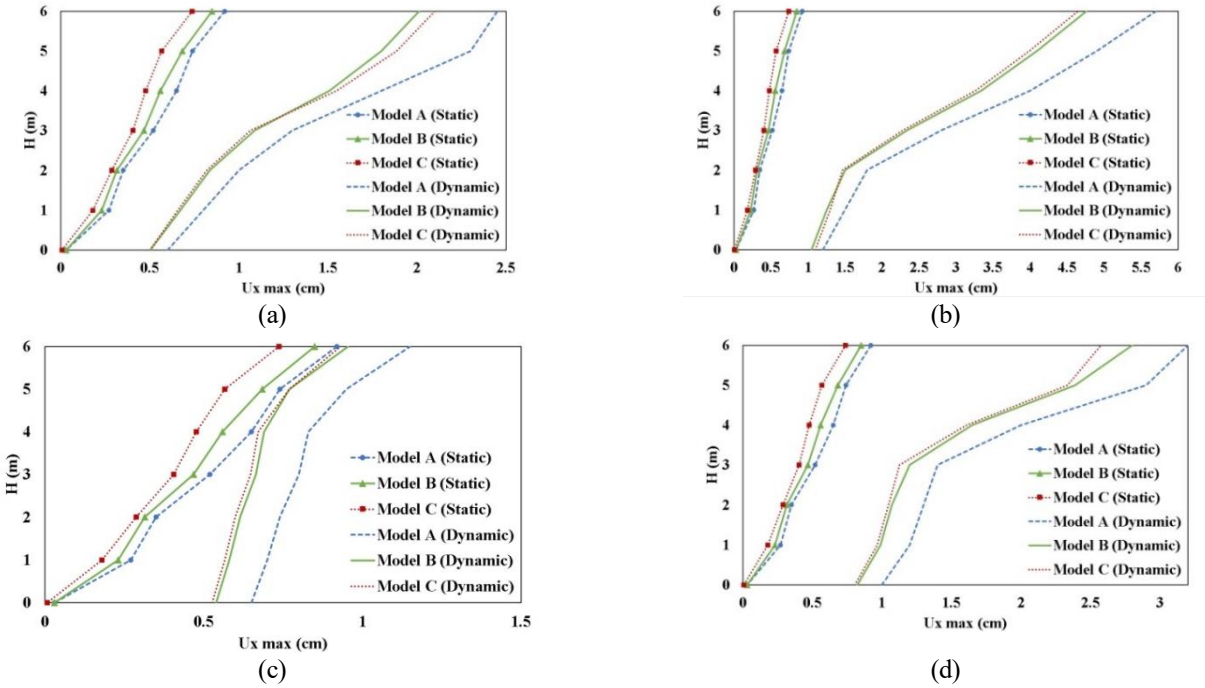

Fig. 8 Comparison of maximum horizontal displacement of the wall in dynamic and static conditions between Model A: Base model, Model B: Increased geogrids number model, and Model C: Increased geogrids stiffness model in the (a) North Palm Spring, (b) Northridge, (c) Kobe and (d) Whittier Narrow earthquakes

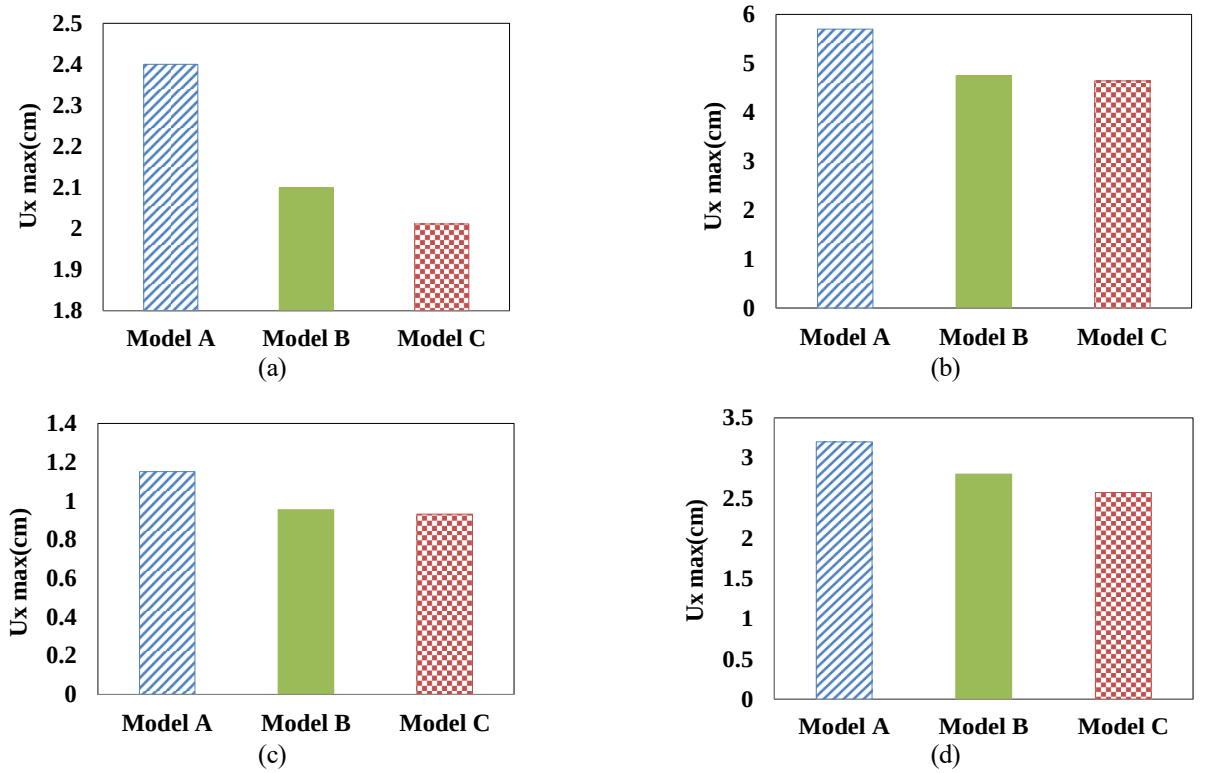

Fig. 9 Bar graphs of SMSEW maximum horizontal displacement in the (a) North Palm Spring, (b) Northridge, (c) Kobe and (d) Whittier Narrow earthquakes, Model A: Base model, Model B: Increased geogrids number model, and Model C: Increased geogrids stiffness model

crest to the foot of the wall under dynamic conditions has increased by 58%, 65%, and 67.5% for Models A, B, and C, respectively. Considering the results, it can be seen that increasing the number and stiffness of geogrids is effective

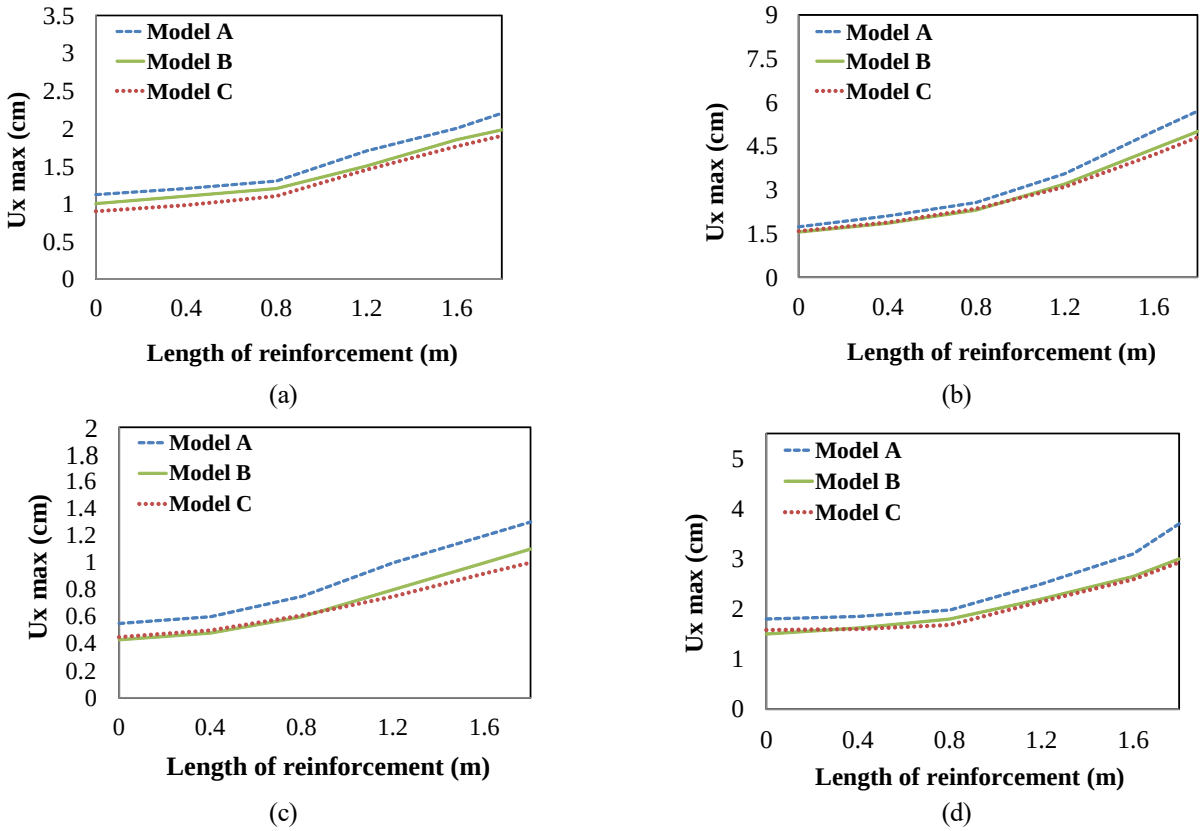

Fig. 10 Comparison of Maximum horizontal displacement along the highest geogrid between A: Base model B: Increased geogrids number model and C: Increased geogrids stiffness model in the (a) North Palm Spring, (b) Northridge, (c) Kobe and (d) Whittier Narrow earthquakes

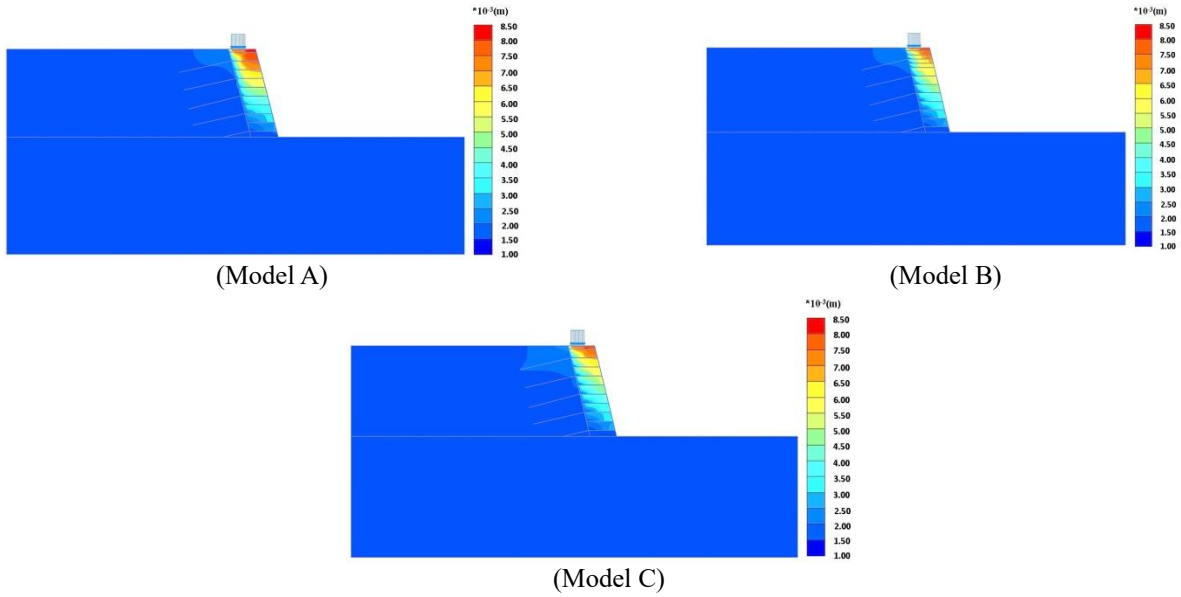

Fig. 11 Comparison of total horizontal displacement (Ux) contours for SMSEW under static conditions between A: Base model B: Increased geogrids number model and C: Increased geogrids stiffness model

in reducing the horizontal displacement of SMSE wall (on average reduction of 16% and 18% for Models B and C, respectively) and improves the efficiency of the wall's performance under seismic loads Fig. 9. Also, Fig. 10 represents the horizontal deformation along the highest geogrid.

As indicated in Fig. 10, in models B and C, the horizontal displacement along the top geogrid from the

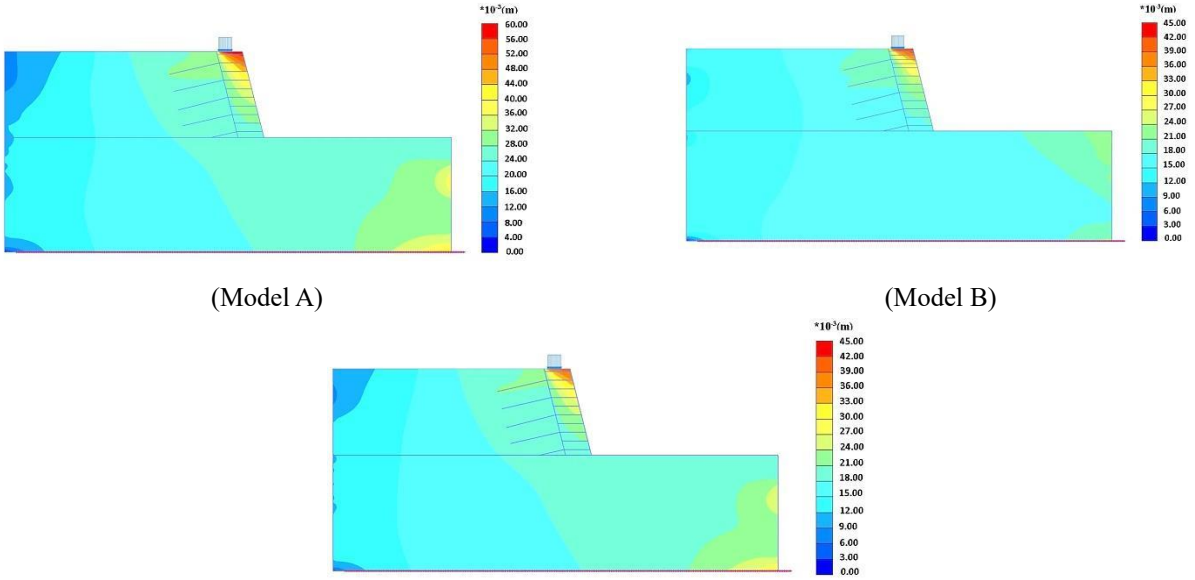

Fig. 12 Comparison of total horizontal displacement (Ux) contours for SMSEW under dynamic conditions (Northridge earthquake) between A: Base Model B: Increased geogrids number model and C: Increased geogrids stiffness model

beginning to the end rises by an average of about 58% and 56%, respectively, which is due to the presence of a shoring wall system at the beginning of the geogrid.

Figs. 11 and 12 illustrate that, in both static and dynamic cases, the peak horizontal displacement of the base model is concentrated at a wall height of 45 cm to 60 cm while, for models B and C, the maximum lateral displacement is observed at a height ranging from 52 cm to 60 cm. This indicates that adding two geogrids on top of the wall and enhancing the geogrids' stiffness effectively reduces the horizontal movement of the SMSE wall, especially under extreme loading conditions like earthquakes.

5. Developing the fragility curves

Fragility curves provide a representation of the likelihood of surpassing a predefined damage level for a specific construction case. This probability can be tailored to a given ground motion intensity level. These curves categorize damage into minor, moderate, extensive, and complete states. They can be separately generated for each damage level, considering various ground motions, and subsequently used as input data for structural damage assessments (Porter 2021). Fragility curves, which are founded on the probability of failure or damage, prove valuable in seismic regions. To assess the vulnerability of different structural elements to earthquake-induced ground motions, one can express the likelihood of reaching or surpassing a specific damage state based on earthquake characteristics such as PGA, PGV, and PGD. Repeating this process for various PGA values or other individual parameters yields normalized curves known as fragility curves (Porter 2021).

To develop the fragility curves, a distribution for the engineering demand parameters (EDP) obtained from nonlinear dynamic analyses must be considered, and the normal distribution is usually used.

Probabilistic techniques are also applied to generate fragility curves, which rely on the outcomes of time history analyses. Typically, fragility curves are constructed by varying the PGA values as the parameter of interest. On this basis, the fragility function can be defined as

$$Fragility = P\left[EDP > AC \middle| IM\right] \tag{2}$$

In Eq. (2), IM represents the Intensity Measure, specifically the PGA value (this study includes PGA values ranging from 0.1 g to 1 g). EDP stands for the Engineering Demand Parameter, which is derived from the results of nonlinear dynamic analyses conducted in this study. AC, on the other hand, corresponds to the Acceptance Criterion, equivalent to the Performance Level outlined in section 5.2. The probability function, given in Eq. (3), can be calculated as

$$P = P\left[EDP > AC\right] = 1 - P\left[EDP < AC\right] = 1 - \phi\left(\frac{AC - \mu}{\sigma}\right) \tag{3}$$

In this study, fragility curves were developed by the analytical method. The framework for developing fragility curves for an SMSE wall is proposed in the following steps:

Step1: Developing a numerical model to predict the seismic response of the SMSE walls.

Step2: Selecting real earthquake ground motions under different Accelerograms for the fragility analysis.

Step3: Calculating the seismic responses of the SMSE walls subjected to selected earthquake events, which are scaled to different levels of ground motion intensity.

Step4: Defining the criteria to damage states of the SMSE walls.

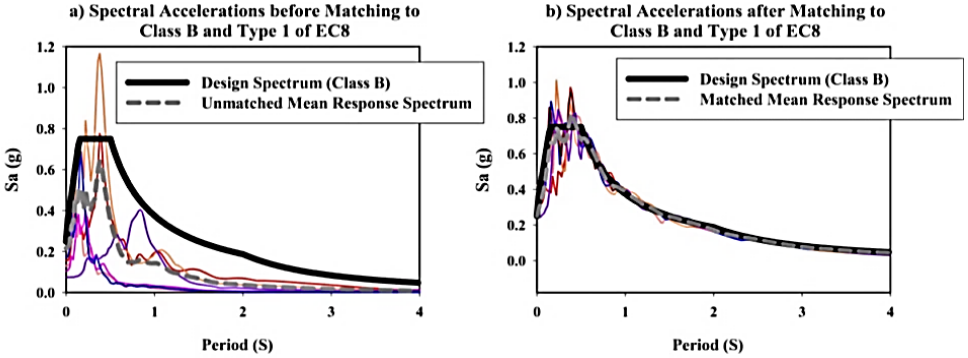

Fig. 13 Matching of the spectral acceleration of the soil class B records for the seven acceleration time histories. (a) Before matching and (b) After matching (for 5% of critical damping)

Table 3 Details of the selected earthquakes based on the site classification of class B in Eurocode 8 (PEER ground motion center)

Event	Station	Record number	Date	R(km)	Mw
Kobe	TOT	PEER:1117	1995/01/16	119	6.9
Loma Prieta	Station Gilroy	CSMIP:47379	1989/10/18	9.64	6.93
N.Palm Springs	Station Silent Valley	CSMIP:12206	1986/07/08	19.5	6.06
Northridge	Station Vasquez	CSMIP:24047	1994/01/17	27.7	6.69
Park field	Temblorpre	USGS:1438	1966/06/28	11.7	6.19
San Francisco	Golden gate Park	USGS:1117	1957/03/22	11.13	5.28
Whittier Narrows	Station Mt Wilson	CSMIP:24399	1987/10/01	22.4	5.99

Step5: Generating the fragility curves through damage probability analysis based on the seismic response data and the set damage criteria.

5.1 Seismic response analysis of SMSE wall

In this study, a consistent set of seismic records was utilized, comprising seven acceleration time histories to develop the fragility curves. These earthquakes were selected based on the PEER ground motion center, as detailed in Table 3.The selection aimed to ensure that seismic parameters, including motion magnitudes, fell within acceptable ranges and possessed suitable frequencies to adequately stimulate the SMSE wall. Consequently, the acceleration and velocity distributions in the PGA and PGV time histories remained within acceptable limits. To standardize the earthquakes' frequency content, a wavelets algorithm proposed by Abrahamson (1992) and Hancock *et al.* (2006) was employed, following European regulations (Eurocode 8), considering stiff soil conditions (Type 1, Soil Class B), as shown in Fig. 13. The study also investigated the influence of various earthquake intensities on structural collapse fragility, considering six levels of earthquake intensities: 0.1 g, 0.2 g, 0.4 g, 0.6 g, 0.8 g, and 1.0 g. For each intensity level, a set of seven accelerograms was applied, and the resulting performance points of the structure due to these selected earthquake events were calculated.

To calculate the seismic response of the SMSE wall, a total of 42 numerical analyses were conducted for SMSE wall models including the base model (validated model), the model with the addition of two geogrids, and the model by increasing the stiffness of the geogrids. These analyses were performed under the influence of earthquakes with six various levels of PGA.

5.2 Defining the criteria for the damage states

One of the important points in presenting fragility curves is defining the damage criteria. Experiences from past earthquakes show that the allowable horizontal deformation of retaining walls is important. Since the allowable horizontal deformation at the top of the wall is commonly used in the engineering literature, in this study, only the residual horizontal displacement of the facing above the wall was used to define the criteria for the damage states. Since no criterion has been presented for the allowable deformation of the SMSE walls, in this study, the allowable horizontal deformation according to the analysis based on the laboratory and experimental research of Yazdandoost (2019) was dedicated. Thus, in the case of wall damage in seismic events, four different damage states including minor, moderate, extensive, and complete failure were identified according to the defined level of damage. The presented results indicate a range of d/H = 0.55-1.10%, representing a transitional state of the walls from the quasi-elastic state to the plastic state, and based on starting the development of active wedge failure, a range of d/H = 5.0%- 5.6%, representing a transitional state of the walls from the plastic state to the failure state, were determined

Table 4 Minimum requirements for damage criteria for MSE/soil nail hybrid retaining walls and definition of damage levels of reinforced soil walls

Level of damage	Residual displacement (cm)	Normalized residual displacement d/H%	Limit state
Minor	3.3	0.55	No damage
Moderate	6.6	1.1	Serviceability limit state (allowed to be used with Care- Plastic deformation boundary)
Extensive	30	5	Restorability limit state (allowed to be used with observation and/or emergency repair failure state boundary)

* d: Residual horizontal displacement on top of the wall, H: Height of the wall (In this study=6 m)

Table 5 Definition of limit states for SMSE walls in road applications

Judgment	$\frac{d}{H}$%	Damage level	Limit state
No limitation in traffic. Restoration is possible in the usual service (a few days).	less than 0.55	Minor Damage	No damage
All vehicles can travel with limitations. Restoration is possible in a short period (a few weeks).	0.55-1.1	Moderate Damage	Serviceability limit state (allowed to be used with Care- Plastic deformation boundary)
It can only be used for emergency purposes. Restoration is possible in a few weeks (1 month).	1.1-5	Extensive Damage	Restorability limit state (allowed to be used with observation and/or emergency repair-failure state boundary)
Total loss of function. Long-term (several months) required for restoration.	Larger than 5	Complete Failure	Ultimate limit state (not allowed to be used)

(Yazdandoust 2019). Table 4 shows the mentioned damage states' boundaries.

Furthermore, varying damage levels for distinct components of the road system infrastructure were delineated, taking into account damage states, performance criteria, and repair costs. To establish these damage levels and exercise engineering judgment, the research by Kuwano *et al*. (2014) served as a reference in this study. These definitions were derived from expert assessments and align with the current study.

As a result, four distinct damage states were identified based on the defined level of damage. These states encompass minor damage, moderate damage, extensive damage, and complete failure.

Table 5 illustrates these states, amalgamating the values proposed by Yazdandoost (2019) and Kuwano *et al*. (2014).

5.3 Generating the fragility curves

The numerical results obtained from Eq. (2) have been used to develop the fragility curve for the considered models. The fragility curves for SMSE walls can be plotted by using the obtained fragility data. Fig. 14 shows three samples of the fragility curves developed for the SMSE wall, including the base model, by adding the number and stiffness of geogrids at different PGA levels. Also, Fig. 15 the percentage of damage probability in three models. As previously mentioned, in this study, the letters of Model A, Model B, and Model C were used to represent the base model, the model by increasing the number of geogrids, and the model by increasing the axial stiffness of geogrids, respectively.

Based on the fragility curves depicted in Figs. 14 and 15, there are three areas of damage states in all three models, and in all cases, the wall has not completely entered the stage of destruction. In the base model, the wider area of the curve is in an extensive damage state compared to other models. Fig. 14 illustrates that the probability of extensive damage decreases with an increase in the number and stiffness of the geogrids (Models B and C). The middle of the fragility curve indicates the earthquake's intensity with a 50% probability of vulnerability of the structure, which is 0.42 in the minor damage state and 0.8 in the moderate damage state for Model A. Also, this value is 0.55 and 0.9, respectively for Model B, and for Model C is 0.5 and 0.95g, respectively. These results show that the vulnerability probability of the SMSE wall reaches 50% when the number of geogrids and the geogrid's stiffness increase. So, stronger acceleration must be applied to the SMSE wall for failure to occur. At the highest ground acceleration coefficient, which was 1g the fragility in the moderate damage state for the base model, by increasing the number of geogrids and increasing the geogrid stiffness was 76%, 62%, and 54%, respectively. These values of fragility were equal to 99%, 98%, and 97% respectively in the case of minor damage. Notably, the probability of complete destruction. was zero percent in all three models. These results show that these walls were less than 1% severely damaged by the earthquake, and over 90% of the walls remained undamaged. Also, Fig. 15 indicates that adding two layers

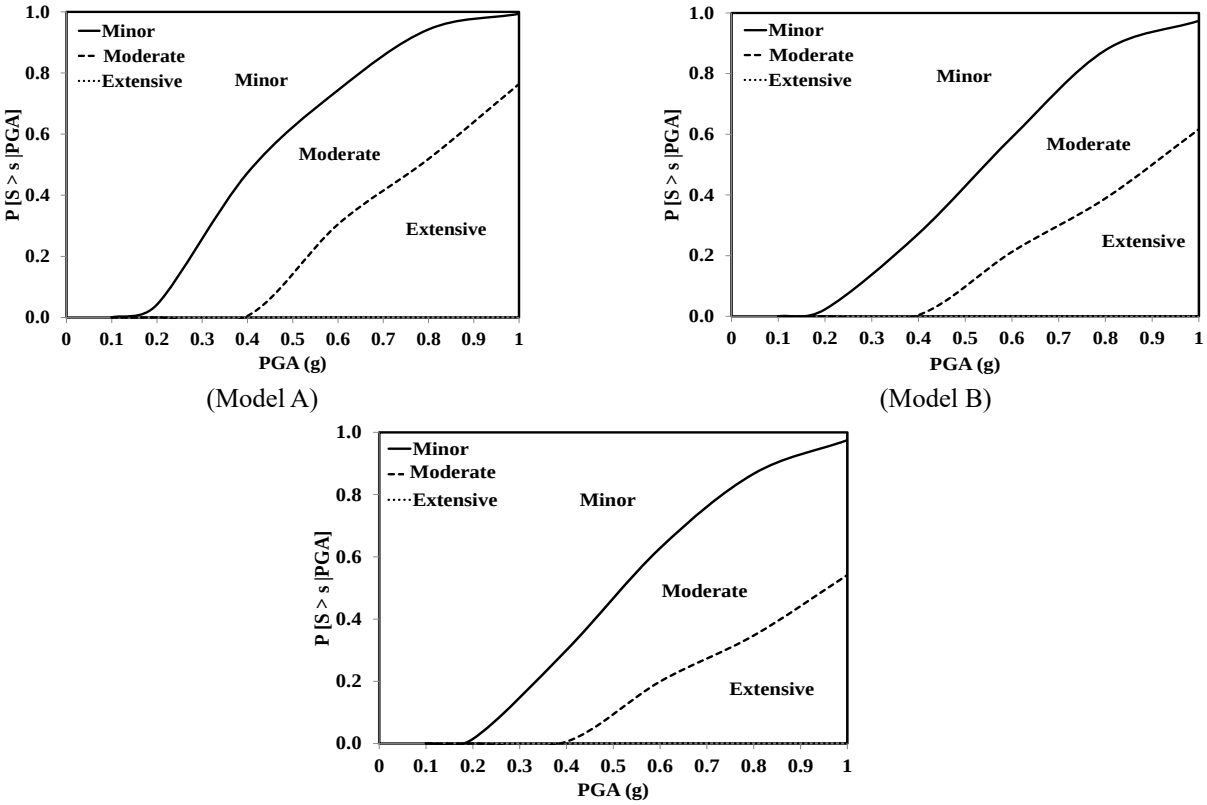

Fig. 14 Fragility curve for SMSE wall in the base model (Model A), model by increasing the number of geogrids (Model B), model by increasing the stiffness of geogrids (Model C)

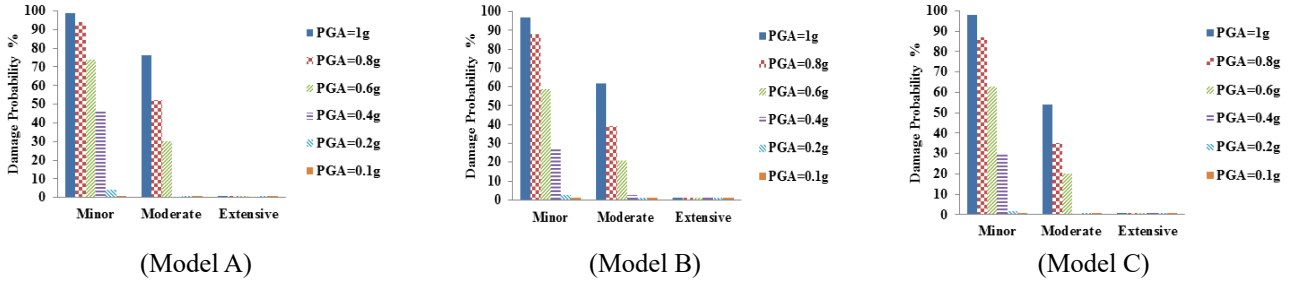

Fig. 15 The percentage of damage probability for the base model (Model A), model by increasing the number of geogrids (Model B), model by increasing the stiffness of geogrids (Model C)

of geogrid and increasing the stiffness of the geogrids is effective in PGA between 0.4 g and 1 g for a moderate damage state and can reduce the probability of vulnerability of the SMSE wall.

5.4 Comparing fragility curves

Fig. 16(a) shows the comparison of the fragility curves between SMSE walls in the case of Models A and B. A notable observation from this comparison is that the SMSE wall with an increased number of geogrids exhibits lower seismic vulnerability than the SMSE wall in the base Model. For instance, at PGA = 0.6 g, the probability of extensive damage state in Model A due to the earthquake is 30%, while the same level of damage in Model B has reached 20%. At PGA =0.8 g, the probability of extensive damage state for Models A and B is 52% and 39%, respectively. Furthermore, the probability of moderate damage state at PGA = 0.4g for models A and B have reached 47% and 27% respectively, as well as in PGA = 0.6 g, these values are 74% and 59%, respectively, and at PGA = 0.8 g for Model A and B have reached 94% and 88%, respectively. These results confirm that the base Model wall is more vulnerable to seismic events than the wall with additional geogrid layers. In other words, increasing the number of geogrids on top of the wall or reducing the vertical distance between them effectively reduces the probability of seismic vulnerability. Notably, the most significant impact of geogrids on seismic vulnerability is within the range of moderate and extensive damage states.

Fig. 16(b) illustrates a comparison of the fragility curves between Models A and C of SMSE walls. The analysis of

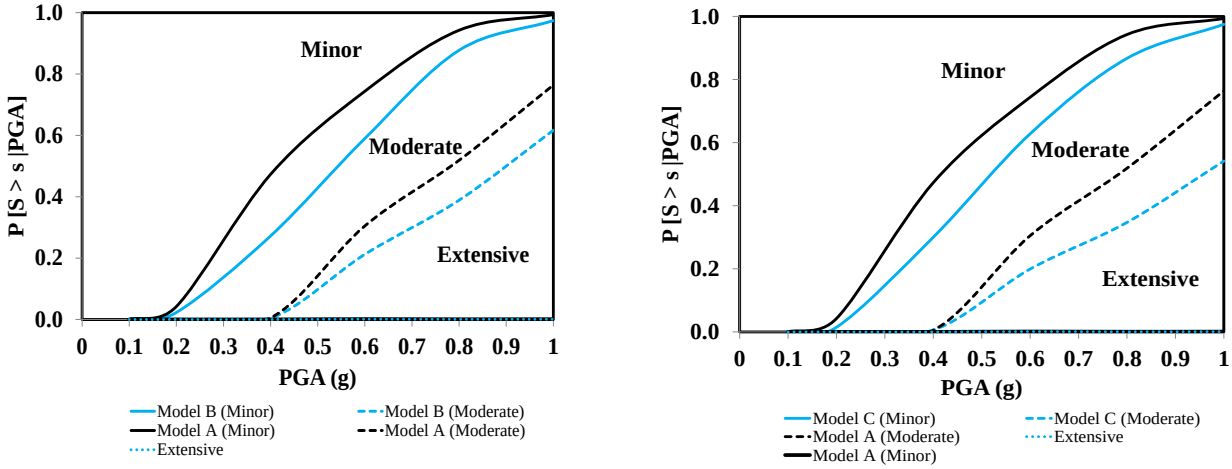

(a) (b)

Fig. 16 Comparison of fragility curves for the two types of SMSE wall (a): (Model A: Base model and Model B: Increased geogrids number model), (b): (Model A: Base model and Model C: Increased geogrids stiffness model)

these curves suggests that the SMSE wall with an increased stiffness of geogrids exhibits lower seismic vulnerability. As can be seen at PGA = 0.6 g, the probability of extensive damage state in Model A due to the earthquake is 30%, but the same level of damage for Model C has reached 21%. At PGA = 0.8 g, the probability of extensive damage state for Models A and C is 52% and 35%, respectively. Also, the probability of moderate damage state at PGA = 0.4 g for Models A and C has reached 47% and 30%, respectively, as well in PGA = 0.6 g, these values are 74% and 63%, respectively, and at PGA = 0.8 g for Models A and C has reached 94% and 87%, respectively. As expected, the SMSE wall with higher stiffness of geogrids reduces the probability of vulnerability. According to the curves, the greatest effect of geogrids on seismic vulnerability is in the range of moderate and extensive damage areas, which indicates that the increased stiffness of geogrids is effective in the probability of seismic vulnerability of this type of wall.

6. Conclusions

Shored mechanically stabilized earth (SMSE) walls represent a modern approach to slope stabilization, offering several advantages over traditional retaining walls. These advantages include support for vehicular traffic during construction, resilience against settlements, enhanced stability and seismic safety, and cost-effectiveness due to shoring walls. Remarkably, there has been a dearth of research on the seismic assessment of SMSE walls, with most studies focusing on static analyses. In response, this study was undertaken to evaluate the seismic vulnerability of SMSE walls during earthquake events and establish fragility curves. These curves provide valuable insights for engineers to anticipate potential structural damage and make informed decisions regarding repairs or reinforcements. To develop fragility curves, we initiated our investigation by conducting numerical finite element method (FEM) simulations using PLAXIS 2D software, employing the HS small soil model. We explored the impact of crucial design parameters, such as geogrid stiffness and quantity. Subsequently, fragility curves were generated for SMSE walls, relying on residual displacements observed during dynamic analyses conducted with selected ground motion records. Our numerical modeling endeavors yielded the following key conclusions:

- The maximum settlement of the embankment surface occurs at the end of the reinforced area, which is decreased by moving away from the facing.
- The maximum horizontal displacement of the wall always occurs at the top of the facing.
- In general, increasing the stiffness of geogrids and adding two geogrids in the upper layers of the wall reduces the horizontal deformation of the wall surface and the facing.
- The horizontal and vertical displacement of the SMSE walls is highly dependent on each earthquake characterization.
- By adding two geogrids in the upper layers of the wall (Model B), the wall's surface settlement is reduced by about 9 to 21 percent.
- Increasing the number of geogrids or reducing the distance between them leads to improved interlock of geogrid networks with soil, resulting in an average 16% reduction in wall surface settlement and enhanced structural performance under seismic loads.
- By increasing the stiffness of the geogrids (up to double) (Model C), the wall's surface settlement is reduced by about 24 to 43 percent.
- Increasing geogrid stiffness leads to an average 34% reduction in wall surface settlement and improved structural performance under seismic loads.
- The maximum wall horizontal displacement versus the wall height in dynamic conditions is 65% for the

base model (Model A) and 60% for Model B by increasing the number of geogrid layers, as well as 57.5% for Model C by increasing the geogrids' stiffness.

- The horizontal displacement along the top geogrid decreases by 58% for the model by increasing two layers of geogrid (Model B) and 56% for Model C by increasing the geogrids' stiffness from the beginning to the end due to the existence of the shoring wall system at the beginning of the geogrid.
- The maximum horizontal deformation of the facing in the highest layer is reduced by about 18% and 20% by adding two geogrids in the upper layers and doubling geogrid stiffness, respectively, compared to the base model.

In the evaluation of the seismic performance of SMSE walls using fragility curves for all three models:

- By adding two geogrids in the upper layers of the wall and increasing the stiffness of the geogrids in the base model, it can be observed that there are three areas of damage state, and one of the walls does not generally enter the complete failure state. Also, in the base model, the wider area of the fragility curves is in an extensive damage state compared to other models.
- At the highest PGA level (1 g), the probability of vulnerability in the moderate damage state is 76% for the base model (Model A), 62% for Model B (increased geogrid layers), and 54% for Model C (increased geogrid stiffness). In the minor damage state, these probabilities are 99%, 98%, and 97%, respectively. The probability of complete destruction is zero percent in all three models.
- The results show that by increasing the number and stiffness of geogrids, the probability of vulnerability of the SMSE wall reaches 50%, and stronger ground acceleration must be applied to the SMSE wall until failure occurs.
- The study shows that these walls experience less than 1% severe damage during an earthquake, with over 90% of the walls showing no damage.
- The study's findings emphasize that enhancing the stiffness of geogrids and adding more geogrid layers significantly lowers the risk of seismic vulnerability in Shored Mechanically Stabilized Earth (SMSE) walls.

According to the results, it can be said that these walls demonstrate stability in dynamic conditions and offer economic advantages, making them a favorable choice, particularly in challenging terrains like steep slopes. However, it's crucial to acknowledge that the fragility curves developed in this research are specific to the studied geometrical and geotechnical conditions. Therefore, these curves and tables should be applied cautiously, considering the unique characteristics of each SMSE wall project.

Funding

The authors received no financial support for the research, authorship, and/or publication of this article.

Acknowledgments

The authors would like to express their great thanks to Mr. Ali Derakhshan for his valuable assistance in editing the manuscript.

References

AASHTO (1995), "AASHTO LRFD bridge design specifications", Washington, D.C.

Abrahamson, N.A. (1992), "Non-stationary spectral matching", *Seismol. Res. Lett.*, **63**(1), 30.

Alhabshi, A. (2006), "Finite element based design procedures for MSE/soil-nail hybrid retaining wall systems", Ph.D. Thesis. Texas, United States: Texas Tech University.

Alielahi, H. and Rabeti Moghadam, M. (2017), "Fragility curves evaluation for broken-back block quay walls", *J. Earthq. Eng.*, **21**(1), 1-22. https://doi.org/10.1080/13632469.2016.1142487.

Altay, G, Kayadelen, C., Çanakci, H., Bagriacik, B., Ok, B. and Oguzhanoglu, M.A. (2021), "Experimental investigation of deformation behavior of geocell retaining walls", *Geomech. Eng.*, **27**(5), 419-431. https://doi.org/10.12989/gae.2021.27.5.419

Argyroudis, S.A., Kaynia, A.M. and Pitilakis, K. (2013), "Development of fragility functions for geotechnical constructions: Application to cantilever retaining walls", *Soil Dyn. Earthq. Eng.*, **50**, 106-116. https://doi.org/10.1016/j.soildyn.2013.02.014.

Bayat, M., Kosarieh, A.H. and Javanmard, M. (2021), "Probabilistic seismic demand analysis of soil nail wall structures using bayesian linear regression approach", *Sustainability*, **13**(11), 5782. https://doi.org/10.3390/su13115782.

Berg, R.R., Christopher, B.R. and Samtani, N.C. (2009), "Design and construction of mechanically stabilized earth walls and reinforced soil slopes", FHWA NHI-10-024 (**Vol. I**) and NHI-10-025 (**Vol. II**). Washington, DC: Federal Highway Administration, US Dept. of Transportation.

Cosentini, R.M. and Bozzoni, F. (2022), "Fragility curves for rapid assessment of earthquake-induced damage to earth-retaining walls starting from optimal seismic intensity measures", *Soil Dyn. Earthq. Eng.*, **152**, 107017. https://doi.org/10.1016/j.soildyn.2021.107017.

Deghoul, L., Gabi, S. and Hamrouni, A. (2020), "The influence of the soil constitutive models on the seismic analysis of pile-supported wharf structures with batter piles in cut-slope rock dike", *Studia Geotechnica et Mechanica*, **42**(3), 191-209. https://doi.org/10.2478/sgem-2019-0050.

El-Emam, M. and Bathurst, R.J. (2006), "Influence of reinforcement parameters on the seismic response of reduced-scale reinforced soil retaining walls", *Geotext. Geomembranes*, **25**(1), 33-49. https://doi.org/10.1016/j.geotexmem.2006.09.001.

Erberik, M.A. (2008), "Fragility-based assessment of typical mid-rise and low-rise RC buildings in Turkey", *Eng. Struct.*, **30**(5), 1360-1374. https://doi.org/10.1016/j.engstruct.2007.07.016.

Eurocode 8: Design of structures for earthquake resistance. (2004), London: British Standards Institution.

Hamrouni, A., Dias, D. and Sbartai, B. (2018), "Reliability analysis of a mechanically stabilized earth wall using the surface response methodology optimized by a genetic algorithm", *Geomech. Eng.*, **15**(4), 937-945. https://doi.org/10.12989/gae.2018.15.4.937.

Hamrouni, A., Sbartai B. and Dias, D. (2021), "Ultimate dynamic bearing capacity of shallow strip foundations - Reliability analysis using the response surface methodology", *Soil Dyn. Earthq. Eng.*, **144**.

https://doi.org/10.1016/j.soildyn.2021.106690.
Hancock, J.J., Watson-Lamprey, N.A., Abrahamson, J.J., Bommer, A., Markatis, E., Maccoy, E.M. and Mendis, R. (2006), "An improved method of matching response spectra of recorded earthquake ground motion using wavelets", *J. Earthq. Eng*., **10**(1), 67-89. https://doi.org/10.1080/13632460609350629.
Huang, Y., Hu, H. and Xiong, M. (2018), "Performance-based seismic fragility analysis of retaining walls based on the probability density evolution method", *Struct. Infrastruct. Eng*., **15**(1). https://doi.org/10.1080/15732479.2018.1520906.
Jafarian, Y. and Miraei, M. (2019), "Scalar-and vector-valued fragility analyses of gravity quay wall on liquefiable soil: Example of Kobe port", *Int. J. Geo. Mech*., **19**, 04019029. https://doi.org/10.1061/(ASCE)GM.1943-5622.0001382.
Jiang, Y., Han, J., Parsons, R.L. and Brennan, J.J. (2016), "Field instrumentation and evaluation of modular-block MSE walls with secondary geogrid layers", *J. Geotech. Geoenviron. Eng.*, **142**(12), 05016002. https://doi.org/10.1061/(ASCE)GT.1943-5606.0001573.
Kamalzadeh, A. and Pender, M.J. (2022), "Dynamic response of Mechanically Stabilised Earth (MSE) structures: A numerical study", *Geotext. Geomembranes*, **51**(2), 73-87. https://doi.org/10.1016/j.geotexmem.2022.09.008.
Kuhlemeyer, R.L. and Lysmer, J. (1973), "Finite element method accuracy for wave propagation problems", *J. Soil Mech. Found. Division*, **99**(5), 421-427. https://doi.org/10.1061/JSFEAQ.0001885.
Kuwano, J., Miyata, Y. and Koseki, J. (2014), "Performance of reinforced soil walls during the 2011 Tohoku earthquake", *Geosynthetics Int*., **21**(3), 179-196. https://doi.org/10.1680/gein.14.00008.
Lee, Y.B., Ko, H.Y. and McCartney, J.S. (2010), "Deformation response of shored MSE walls under surcharge loading in the centrifuge", *Geosynthetics Internationa*, **17**(6), 389-402. https://doi.org/10.1680/gein.2010.17.6.389.
Ling, H., Leshchinsky, D. and Chou, N.N.S. (2001), "Post-Earthquake Investingation walls and slopes during the Ji-Ji Earthquake of Taiwan", *Soil Dyn. Earthq. Eng*., **21**(4), 297-313. https://doi.org/10.1016/S0267-7261(01)00011-2.
Morrison, K.F., Harrison, F.E., Collin, J.G., Dodds, A. and Arndt, B. (2006), "Shored Mechanically Stabilized Earth (SMSE) wall systems design guidelines", FHWA-CFL/TD-06-001. Washington, DC: Federal Highway Administration, US Dept. of Transportation.
PEER (Pacific Earthquake Engineering Research) (2010), "PEER ground motion database", University of Berkeley, California. https://peer.berkeley.edu/peer-strong-ground-motion-databases.
Payeur, J., Corfdir, A. and Bourgeois, E. (2015), "Dynamic behavior of a mechanically stabilized earth wall under harmonic loading: Experimental characterization and 3D finite elements model", *Comput. Geotech.*. **65**, 199-211. https://doi.org/10.1016/j.compgeo.2014.12.001.
PLAXIS 2D Reference Manual (2020), https://communities.bentley.com/manuals.
Raslan Alainia (2019), Developing Fragility Curves for Earth-Retaining walls due to Dynamic loads, Master Thesis, Politecnico Di Torino.
Ren, F.F. and Qi, M.X. (2017), "Model tests on the shored mechanically stabilized earth wall", *Proceedings of the 6th National Symposium on Geosynthetics and Reinforced Earth*, Shanghai, China.
Ren, F.F., Xu, H., Ji, Y.J., Huang, Q.Q. and Tian, X. (2022). "Experimental study on the mechanical behavior of shored mechanically stabilized earth walls for widening existing reinforced embankments", *Geotext. Geomembranes*, **50**(3), 737-750. https://doi.org/10.1016/j.geotexmem.2022.03.013.
Ren, F.F., Hao, Q. and Wang, G. (2019), "Numerical comparison on deformation characteristics of the shored mechanically stabilized earth wall between reduced-scale and full-scale models", *Soil Mech. Found. Eng.*, **56**(5), 302-308. https://doi.org/10.1007/s11204-019-09606-6.
Safaee, A.M., Mahboubi, A. and Noorzad, A. (2021), "Experimental investigation on the performance of multi-tiered geogrid mechanically stabilized earth (MSE) walls with wrap-around facing subjected to earthquake loading", *Geotext. Geomembranes*, **49**(1), 130-145. https://doi.org/10.1016/j.geotexmem.2020.08.008.
Samtani, N.C. and Alexander, D.E. (2005), "Remediation of a failing MSE wall by Jet grouting", Geo-Frontiers Congress, https://doi.org/10.1061/40783(162)24.
Sandri, D. (1994), "Retaining wall stand up to the Northridge earthquake", *Geotechnical Fabric Reports*, **12**(4), 30-31.
Seo, H., Lee, Y.J., Park, D. and Kim, B. (2022), "Seismic fragility assessment for cantilever retaining walls with various backfill slopes in South Korea", *Soil Dynam. Earthq. Eng*., **161**, 107443. https://doi.org/10.1016/j.soildyn.2022.107443.
Suppasri, A., Koshimura, S. and Imamura, F. (2011), "Developing tsunami fragility curves based on the satellite remote sensing and the numerical modeling of the 2004 Indian Ocean tsunami in Thailand", *Natural Hazards and Earth System Sciences*. **11**(1), 173-189. https://doi.org/10.5194/nhess-11-173-2011, 2011.
Tatsuko, F., Koseki, J., Tateyama, M. and Horii, K. (1995), "Performance of geogrid reinforced soil retaining walls during the grate Hanshin-Avaji earthquake", *International conference on earthquake geotechnical engineering*, **2**, 55-62.
Turkel, B., Yildirim, I.Z. and Guler, E. (2020), "The effect of natural frequency on the seismic behavior of an 8 m high MSE wall", Geo-Congress. GSP 316. https://doi.org/10.1061/9780784482797.040.
Xie, Y. and Leshchinsky, B. (2015), "MSE walls as bridge abutments: Optimal reinforcement density", *Geotext. Geomembranes*, **43**(2), 128-138. https://doi.org/10.1016/j.geotexmem.2015.01.002.
Xu, P., Hatami, K. and Jiang, G. (2020), "Study on seismic stability and performance of reinforced soil walls using shaking table tests", *Geotext. Geomembranes*, **48**(1), 82-97. https://doi.org/10.1016/j.geotexmem.2019.103507.
Xu, P., Hatami, K. and Jiang, G. (2021a), "Shaking table performance of reinforced soil retaining walls with different facing configurations", *Geotext. Geomembranes*, **49**(3), 516-527. https://doi.org/10.1016/j.geotexmem.2020.10.003.
Xu, P., Hatami, K. and Jiang, G. (2021b), "Shaking table study on the influence of ground motion frequency on the performance of MSE walls", *Soil Dyn. Earthq. Eng*., **142**(4), 106585. https://doi.org/10.1016/j.soildyn.2021.106585.
Xu, P., Y. Zhong, K. Hatami, G. Yang, W. Liu, G. Jiang. (2023). "Influence of reinforcement design on seismic stability of full-height panel MSE walls", *Soil Dyn. Earthq. Eng.*, **165**. https://doi.org/10.1016/j.soildyn.2022.107674.
Yang, K.H., Zornberg, J.G., Hung, W.Y. and Lawson, C.R. (2011), "Location of failure plane and design considerations for narrow geosynthetic reinforced soil wall systems", *J. Geo. Eng.*, **6**(1), 27-40. https://doi.org/10.6310/jog.2011.6(1).3.
Yazdandoust, M. (2017), "Investigation on the seismic performance of steel-strip reinforced-soil retaining walls using shaking table test", *Soil Dyn. Earthq. Eng*., **97**, 216-232. https://doi.org/10.1016/j.soildyn.2017.03.011.
Yazdandoust, M. (2019), "Shaking table modeling of MSE/soil nail hybrid retaining walls", *Soils Found.*, **59**(2), 241-252. https://doi.org/10.1016/j.sandf.2018.05.013.
Yuu, J., Han, J., Rosen, A., Parsons, R.L. and Leshchinsky, D. (2008), "Technical review of geocell-reinforced base courses over weak subgrade", The First Pan American Geosynthetics

Conference & Exhibition proceedings (GeoAmericas), Appendix VII, Cancun, Mexico. 1022-1030.
Zamiran, S. and Osouli, A. (2018), "Seismic motion response and fragility analyses of cantilever retaining walls with cohesive backfill", *Soils Found.*, **58**(2), 412-426. https://doi.org/10.1016/j.sandf.2018.02.010.
Zhang, X.W. (2017), "Scale model test of the behavior of the shored mechanically stabilized earth (SMSE) wall", Ba. Thesis. Shanghai, China: Tongji University.
Zheng, Y., Li, F., Guo, W.,Wang, P. and Yang, G. (2023), "Influence of facing conditions on the dynamic response of back-to-back MSE walls", *Soil Dyn. Earthq. Eng.*, **164**. https://doi.org/10.1016/j.soildyn.2022.107650.

GC